



Effect of endohedral nickel atoms on the hydrophilicity of carbon nanotubes

Shakhrizoda Matnazarova^a, Umedjon Khalilov^{b,c,d,a} and Maksudbek Yusupov^{e,d,a,f}

^aArifov Institute of Ion-Plasma and Laser Technologies, Academy of Sciences of Uzbekistan, Tashkent, Uzbekistan; ^bCentral Asian University, Tashkent, Uzbekistan; ^cTashkent International University of Education, Tashkent, Uzbekistan; ^dNational Research University TIIAME, Tashkent, Uzbekistan; ^eNew Uzbekistan University, Tashkent, Uzbekistan; ^fUniversity of Antwerp, Antwerp, Belgium

ABSTRACT

Carbon nanotubes (CNTs) have been successfully used in biomedicine, including cancer therapy, due to their unique physico-chemical properties. Because pristine CNTs exhibit hydrophobic behaviour, they can have a cytotoxic effect on cells, which limits their practical use in biomedicine. The toxicity of CNTs can be reduced by adding water-soluble functional radicals to their surface, i.e. by increasing their hydrophilicity. Another possibility for increasing the hydrophilicity of CNTs is probably filling them with endohedral metal atoms, which has not yet been studied. Thus, in this study, we use computer simulations to investigate the combined effect of endohedral nickel atoms and functional groups on the hydrophilicity of CNTs. Our simulation results show that the introduction of endohedral nickel atoms into CNTs increases their binding energy with functional groups. We also find that the addition of functional groups to the surface of CNT, along with filling it with endohedral nickel atoms, leads to an increase in the dipole moment of the CNT as well as its interaction energy with water, thereby increasing the hydrophilicity of the CNT and, consequently, its solubility in water. This, in turn, can lead to a decrease in CNT toxicity.

ARTICLE HISTORY

Received 14 June 2023
Accepted 22 August 2023

KEYWORDS

Single-walled carbon nanotubes; functional groups; endohedral nickel atoms; molecular dynamics

1. Introduction

Carbon nanostructures possess distinctive physical, chemical, and biological properties, making them highly promising materials employed across various fields [1]. Among them, carbon nanotubes (CNTs) are increasingly utilized due to their extraordinary electrical and mechanical characteristics [2]. In the field of biomedicine, CNTs have found applications in the efficient transport and delivery of biological drugs, as well as in biosensing technologies [3–7]. These nanotubes serve as membrane channels within cells, demonstrating remarkable capabilities for transporting DNA and facilitating drug delivery across cell membranes [8–11]. Particularly in cancer treatment, CNTs have emerged as promising carriers [12]. Their utilization helps mitigate the adverse effects of therapy, such as drug toxicity [12–15], while simultaneously enabling targeted drug delivery to tumor sites [16]. Consequently, this approach minimizes damage to healthy tissues in patients.

CNTs exhibit hydrophobic characteristics attributed to their sp^2 -hybridized carbon structure. Consequently, they tend to aggregate when placed in aqueous solutions [17] due to their insolubility in water [18,19]. The hydrophobic nature of the surface of these aggregated CNTs leads to a specific chemical binding of essential nutrients crucial for cell growth, resulting in an indirect cytotoxic effect on cells characterized by cellular damage and death [20]. Notably, experiments conducted on animal models have demonstrated an increase in cases of CNT-induced lung toxicity [21,22]. These observations pose limitations on the practical application of CNTs in biomedicine, necessitating the reduction of their toxicity through the enhancement of their solubility in aqueous environments [23].

One effective approach to mitigate the toxicity of CNTs involves their surface modification with biocompatible organic materials, specifically water-soluble functional radicals. Remarkably, experimental investigations utilizing CNTs functionalized with carboxyl ($-COOH$) radicals have demonstrated non-cytotoxic effect of these functionalized CNTs (fCNTs) [24]. Additionally, numerous studies have highlighted a substantial improvement in the solubility of CNTs following their modification with functionalized groups [23,25–30]. Quantum mechanical calculations have specifically indicated that an increase in the number of functional groups on the surface of carboxylated single-walled CNTs (SWNTs) leads to elevated Gibbs free energy of solvation and dipole moments of SWNTs [23], resulting in increased solubility of SWNTs in water [23].

In addition to functional groups, the incorporation of endohedral transition metal atoms into the nanotube structure [31,32] has the potential to alter its surface properties, such as hydrophilicity, leading to consequential effects on its solubility. However, to the best of our knowledge, no previous research has investigated the specific influence of endohedral transition metal atoms, as well as their combined effect with functional groups, on the hydrophilicity of CNTs. Therefore, to address this research gap comprehensively, we conduct molecular dynamics (MD) simulations to examine the impact of endohedral nickel (Ni) atoms on the hydrophilic properties of SWNTs. In this context, the aim of this study is to gain valuable insight into the synergistic effect between endohedral transition metal atoms and functional groups, with a particular focus on how they collectively affect the hydrophilicity of SWNTs.

2. Simulation details

Atomic-scale reactive MD simulations were performed to investigate the interaction mechanisms of pristine SWNT (pSWNT) and functionalized SWNT (fSWNT) (with and without endohedral Ni atoms) with water by applying the ReaxFF force field [33]. This force field has been used to study the properties of various model systems, including water [34] and CNT [35]. In this study, we used the parameter set of ReaxFF developed by Zou et al. [36]. This set of parameters has been shown by Khalilov et al. to describe the CNT very well (i.e. accurately and reliably) [35]. To verify whether it can describe the water environment well enough, we carried out additional MD simulations. For this purpose, a model system consisting of 500 water molecules placed in the simulation box with dimensions of $25 \times 25 \times 23.93 \text{ \AA}^3$ and periodic boundary conditions were applied in all Cartesian directions (i.e. x, y and z). It was determined that under this condition, water obtained a density of 1 g/cm^3 . The energy of the model system was minimized using the conjugate gradient method. Then, the system was heated to a temperature of 300 K for 300 ps using the Berendsen thermostat [37] with dumping constants of 0.1 ps by applying the NVT ensemble. Using the thermalized water system, several quantities representing its properties (e.g. O-H bond and HOH angle in water) were determined (see below), thus confirming the reliability of the ReaxFF parameter set used in this work.

To study the properties of CNTs, we first created a pSWNT (Figure 1a) with chirality (5,5), a length of 22 \AA and a diameter of 6.8 \AA using Nanotube Modeler software. The average length of carbon-carbon (C-C) bonds in this nanotube was 1.43 \AA , which is consistent with the SWNT parameters obtained in the literature [35]. To form fSWNT model systems, one, two and three carboxyl (-COOH) radicals were covalently bonded to the surface of pSWNT (see Figure 1b-d). These functional groups were connected to the middle areas of SWNT in the direction of the z-axis.

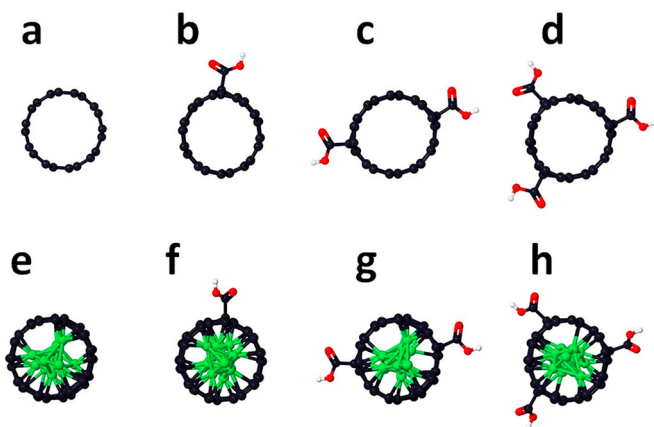


Figure 1. Top view of pSWNT with (5,5) chirality (a) and its functionalized forms with one (b), two (c) and three (d) carboxyl (-COOH) radicals. The same structures filled with endohedral Ni atoms (e-h). Carbon, oxygen, hydrogen, and nickel atoms are shown in black, red, white, and green, respectively.

To create SWNT model systems with endohedral Ni atoms, we introduced 18 Ni atoms into the above mentioned nanotubes (Figure 1e-h). Note that this number of Ni atoms corresponded to approximately 97% of the inner volume of the SWNT, which was calculated using the concept of the effective diameter [38], i.e. $d_{\text{eff}} = d_{\text{geo}} - \sigma_{\text{C-Ni}}$, where d_{eff} is the effective diameter of the SWNT, d_{geo} is the geometric diameter of the SWNT (i.e. 6.93 \AA), and $\sigma_{\text{C-Ni}}$ is the sigma bond length of C-Ni (i.e. 2.5 \AA). These 8 model systems were then placed in a simulation box with a size of $22 \times 22 \times 22.2 \text{ \AA}^3$. Periodic boundary conditions were applied along the three directions of the simulation box, which allowed the SWNTs to be considered long enough to mimic the experimental studies. Initially, the energy of the model systems was minimized using the conjugate gradient method. Then, the temperature of the systems was gradually increased to 300 K (with a heating rate of 1 K/ps) using the NpT ensemble under a pressure of 1 atm for 300 ps. To control the temperature and pressure of the systems, the Berendsen thermostat and barostat were applied with corresponding dumping constants of 0.1 and 5 ps, respectively [37]. Subsequently, the temperature of the model systems was kept for 300 ps using the Berendsen thermo-barostat in the NpT ensemble. A time step of 0.25 fs was chosen in all MD simulations.

To study the interaction of water with SWNTs, these eight model systems were surrounded by water molecules and placed in the same simulation box as mentioned above (i.e. $22 \times 22 \times 22.2 \text{ \AA}^3$). Subsequently, all the above steps (i.e. minimization and thermalization) were performed to create well-equilibrated model systems in a water environment. To calculate the average dipole moments of all eight model systems, we used 600 MD frames extracted from the last 150 ps of the simulations.

The investigation of binding energy barriers associated with functional radicals is interesting [39], as it provides insights into the influence of endohedral Ni atoms on these barriers. Consequently, to evaluate the binding energy barriers of functional radicals on the surface of SWNTs, we employed the nudged elastic band (NEB) method [40]. For this purpose, we extracted 10 frames from MD simulations of SWNT structures over the final 150 ps (at 15 ps intervals). These MD frames included SWNTs with one, two, and three functional radicals, resulting in a total of 30 configurations. These chosen configurations were then adopted as the final (i.e. bound) states in the NEB calculations. To create configurations with initial (i.e. unbound) states, we placed each functional radical approximately 11 \AA from the surface of the selected SWNTs. Consequently, a total of 60 structures were employed for NEB calculations: 10 configurations with one functional radical, 20 with two, and 30 with three functional radicals, respectively. The determined binding energy barriers were subsequently averaged to obtain the final binding energy barrier for each configuration (i.e. SWNTs with one, two and three functional radicals). The same procedure was applied to SWNT structures with endohedral Ni atoms, again using 60 configurations (see above). Thus, in total, 120 NEB calculations were conducted to determine the average binding energy barriers.

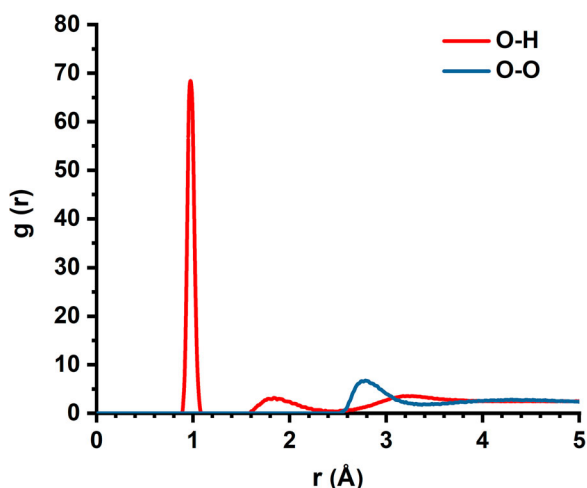


Figure 2. RDF of distances between O-H and O-O atoms of water molecules.

2.1. Results and discussion

2.1.1. Force field validation

To validate the accuracy of the ReaxFF force field (namely, its parameter set developed by Zou et al. [36]) for the water model system, a number of parameters related to water, i.e. the average O-O and O-H distances in water molecules and their radial distribution functions (RDFs), the average HOH angle of water and OH-O angle formed due to hydrogen bonds, partial charges of O and H atoms (δ_{O} and δ_{H}), and the average dipole moment of water molecules (μ), were calculated. Figure 2 illustrates the RDFs of O-O and O-H distances.

As can be seen from the figure, two peaks for O-H are found at distances of 0.96 and 1.83 Å (shown in red). These distances correspond to the lengths of the O-H bonds in the water molecule and the O-H hydrogen bonds formed between water molecules, respectively. For the O-O distance (shown in blue), only one peak is observed at 2.78 Å, which corresponds to the distance between the O atoms of the two nearest water molecules. The results of these RDFs are consistent with other findings in the literature [41]. In Table 1, the parameters of the water molecule calculated in this study are compared with those reported in the literature.

As seen from the table, the O-H and O-O distances determined in this study agree with the distances calculated earlier by Fogarty et al. [41] (column 3) and are very close to the SPC (column 4), *ab initio* (column 5) and experimental (column 6) results. A similar conclusion can be drawn about the HOH angle, except for SPC; this angle is slightly larger than that of the others. The calculated OH-O angle is somewhat smaller than the previous one and calculated from first principles and

experiments but still close (i.e. within the error) to the ReaxFF results in column 3. The partial charge results of this study are also almost identical to the previous ReaxFF results. Regarding the dipole moment, the results of this research are very close to the results of ReaxFF in column 3 and lie within the range of values in other results. In general, our simulation results for water parameters are almost consistent with other results of classical [41,42] and quantum mechanical [43] calculations, as well as experiments [44–48]. Thus, the ReaxFF force field parameters developed by Zou et al. [36] used in this study can be employed to describe the water environment.

We also conducted RDF calculations for C-C distances in both SWNTs with and without endohedral Ni atoms to examine the influence of Ni atoms on these lengths, as illustrated in Figure 3. In Figure 3a, three distinct C-C distances, labelled as d_1 , d_2 , and d_3 , are evident within a radius of 3.25 Å. The corresponding RDF of them is depicted in Figure 3b. For SWNTs without endohedral Ni atoms, the peaks for these C-C distances appear at 1.42, 2.45, and 2.83 Å (cyan colour). In the case of SWNTs with endohedral Ni atoms, these peaks undergo slight shifts to approximately 1.43, 2.46, and 2.85 Å (blue colour). The observed shifts are likely attributed to Coulomb interactions between the Ni and C atoms, which induce a subtle elongation in the SWNT C-C bonds, resulting in a slight overall increase in the above-mentioned C-C distances.

2.1.1.1. Binding of functional groups (-COOH) with SWNT.

To evaluate the interaction of hydrophilic functional groups with nanotubes, the binding energy E_b of these groups to the surface of SWNT was calculated, which is determined as follows:

$$E_b = E_{\text{SWNT}-(\text{COOH})_n} - (E_{\text{SWNT}} + E_{(\text{COOH})_n}) \quad (1)$$

where n is the number of functional groups ($n = 1-3$), $E_{\text{SWNT}-(\text{COOH})_n}$ is the potential energy (eV) of the system consisting of SWNT and functional group(s), and E_{SWNT} and $E_{(\text{COOH})_n}$ are the potential energies (eV) of SWNT and functional group(s), respectively. Thus, using formula (1), we calculated the binding energy of the -COOH radical(s) with the SWNT surface under vacuum conditions (see Figure 4). As is clear from Figure 4, in SWNTs without endohedral Ni atoms, the average binding energy corresponding to one radical practically does not change with an increase in the number of radicals. Specifically, the binding energy corresponding to one radical is equal to -4.63, -4.63 and -4.60 eV for SWNTs with one, two and three functional groups, respectively.

Table 1. Comparison of water parameters calculated in this study with those available in the literature.

| parameters | ReaxFF-Zou (this study) | ReaxFF-van Duin ^a | SPC/E ^b | <i>ab initio</i> BLYP ^c | experiments |
|-------------------------|-------------------------|------------------------------|--------------------|------------------------------------|---------------------|
| O-H distance (Å) | 0.98 ± 0.05 | 0.98 ± 0.04 | 1.00 | 0.97 | 0.96 ^d |
| O-O distance (Å) | 2.88 ± 0.20 | 2.88 ± 0.20 | ... | 2.95 | 2.98 ^e |
| HOH angle (°) | 104.50 ± 0.01 | 104.00 ± 4.00 | 109.47 | 104.40 | 104.50 ^f |
| OH-O angle (°) | 164.00 ± 1.29 | 168.00 ± 6.00 | ... | 173.00 | 174.00 ^g |
| δ_{O} (e) | -0.73 ± 0.00 | -0.73 ± 0.03 | -0.85 | ... | ... |
| δ_{H} (e) | 0.37 ± 0.00 | 0.36 ± 0.03 | 0.42 | ... | ... |
| μ (D) | 2.12 ± 0.01 | 2.10 ± 0.20 | 2.35 | 1.81 | 2.90 ^h |

^{a-h} - [41–48]

Previous quantum mechanical calculation results showed that the increase in the number of radicals on the surface of SWNT leads to a decrease in their binding energy to SWNT (i.e. weakening of the bond) [23]. The difference between the results of this work and the results of quantum mechanical calculations can be explained by the size of the SWNT and the hydrogen termination of its edges. In other words, in the quantum mechanical study, a model SWNT structure with a finite length of 8.65 Å was chosen, and the edges of the nanotube were completely terminated by hydrogen atoms [23]. The interaction of these hydrogen atoms with the functional groups in SWNT through nonbonding (i.e. van der Waals and Coulomb) forces can affect the binding energy of these groups with SWNT. In our research, the absence of hydrogen atoms in the structure of SWNT eliminates the possibility of their interaction with functional groups, and therefore, the binding energy does not change (see Figure 4, green curve). In addition, the sufficiently long length (~22 Å) of SWNT prevents them from interacting with functional groups even if there are hydrogen atoms on its edges (i.e. hydrogen atoms and functional groups are outside the cutoff radius of interactions, i.e. 10 Å). Indeed, our test simulations with sufficiently long (~22 Å) SWNT structures terminated with hydrogen atoms fully confirmed our above hypothesis. Namely, the binding energy corresponding to a single radical in a vacuum environment was equal to -4.61, -4.62 and -4.59 eV for terminated SWNTs with one, two and three functional groups, respectively. In the case of SWNTs with endohedral Ni atoms (Figure 4, orange curve), the binding energy corresponding to one radical decreases slightly with an increase in the number of radicals. In particular, the binding energy corresponding to one radical is equal to -5.15, -5.05 and -5.00 eV for SWNTs with one, two and three functional groups, respectively. However, taking into account the standard deviations, one can conclude that these values are still very close (see Figure 4, orange curve). It is also clear that these energy values are slightly (~1.1 times) higher than those of SWNTs without endohedral Ni atoms, which

indicates a stronger binding of functional groups to the SWNT surface upon introduction of endohedral Ni atoms. This can be explained by the fact that endohedral Ni atoms lead to a change in the partial charges of SWNT C atoms due to the Coulomb interactions between Ni and C atoms.

To assess the influence of endohedral Ni atoms on the binding energy barrier (ΔE_b) between hydrophilic functional groups and nanotubes, we calculated these binding energy barriers using the NEB method. Figure 5 shows the average binding energy barrier of a single functional radical on SWNTs with and without endohedral Ni atoms.

It is evident from figure that for SWNTs without endohedral Ni atoms, the binding energy barrier corresponding to one radical practically does not change with an increase in the number of radicals (i.e. about 1.46 eV), especially when standard deviations are taken into account (see Figure 5, yellow bars). In the case of SWNTs with endohedral Ni atoms, for all three structures, somewhat higher energy barriers are observed, which increase with an increase in the number of radicals. Specifically, the binding energy barrier corresponding to one radical is equal to -1.52, -1.61 and -1.88 eV for SWNTs with one, two and three functional groups, respectively (see Figure 5, blue bars). Thus, the introduction of endohedral Ni atoms into SWNTs results in a slight increase in the average energy barrier for binding the functional radical to the SWNT surface. Nevertheless, considering the associated standard deviations, we can conclude that all these energy barriers are still relatively close to each other (see Figure 5).

2.1.1.2. Dipole moment of SWNT. By examining the dipole moment of pristine/functionalized nanotubes with and without endohedral Ni atoms, one can estimate the change in their solubility in a solvent. Thus, we calculated the dipole moments of all eight SWNTs (see Figure 1) in a water environment. Figure 6 shows the average dipole moments of all SWNTs as a function of the number of functional groups (i.e. -COOH radicals).

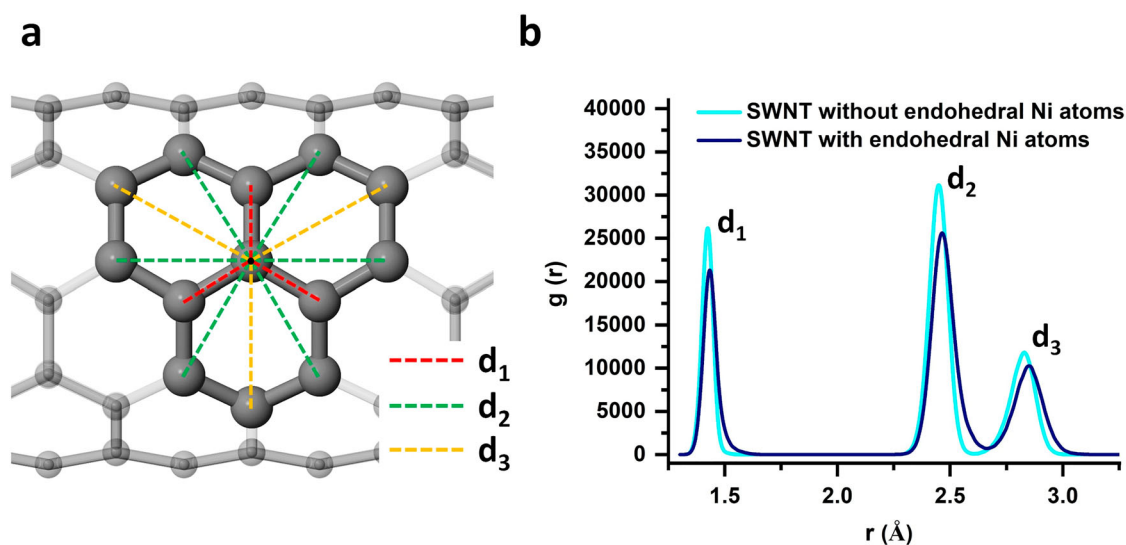


Figure 3. (a) Three different C-C distances, denoted as d_1 , d_2 and d_3 , within a radius of 3.25 Å from the central carbon atom and (b) their respective RDFs for SWNTs with and without endohedral Ni atoms.

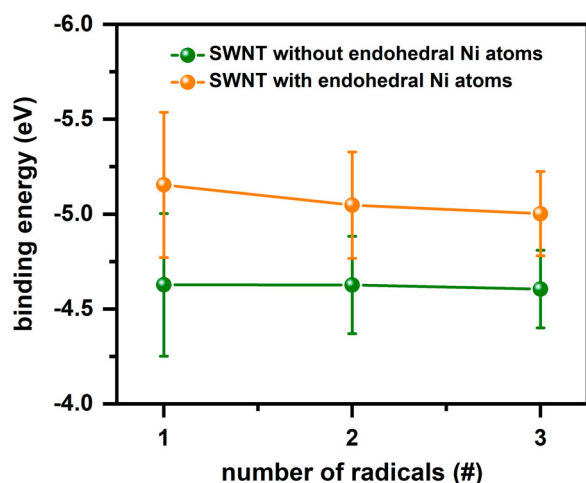


Figure 4. Average binding energy of the -COOH radical to the SWNT surface with (orange) and without (green) endohedral Ni atoms as a function of the number of functional groups (i.e. -COOH radicals). Associated standard deviations are shown as error bars.

As is obvious, functionalization of pSWNT with -COOH radicals significantly increases its average dipole moment. In particular, the average dipole moments of pSWNT and fSWNT without endohedral Ni atoms containing one, two and three -COOH radicals are 0.001, 3.793, 1.946 and 1.541 D, respectively (see green bars in Figure 6). It is clear that the average dipole moment of pSWNT is almost 0 D, indicating that pSWNT is insoluble in polar solvents such as water [23]. The main reason for this is that the calculated partial charges of the C atoms of pSWNT are almost zero. A decrease in the average dipole moment with an increase in the number of functional groups can probably be explained by the fact that the dipole moments of the functional groups remain in opposite directions, thereby attenuating each other. In the case of SWNT filled with endohedral Ni atoms and functionalized with -COOH radicals, the average dipole moment increases significantly compared to that of pSWNT (see orange bars in

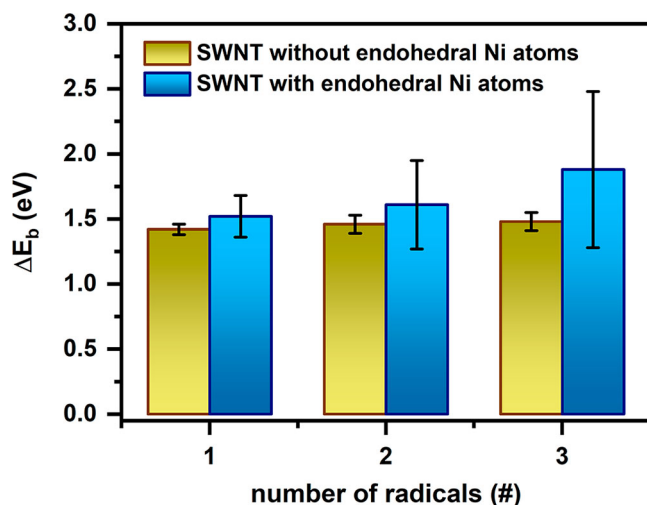


Figure 5. Average energy barrier of -COOH radical binding to the surface of SWNTs with and without endohedral Ni atoms, depending on the number of functional groups (i.e. -COOH radicals). Associated standard deviations are shown as error bars.

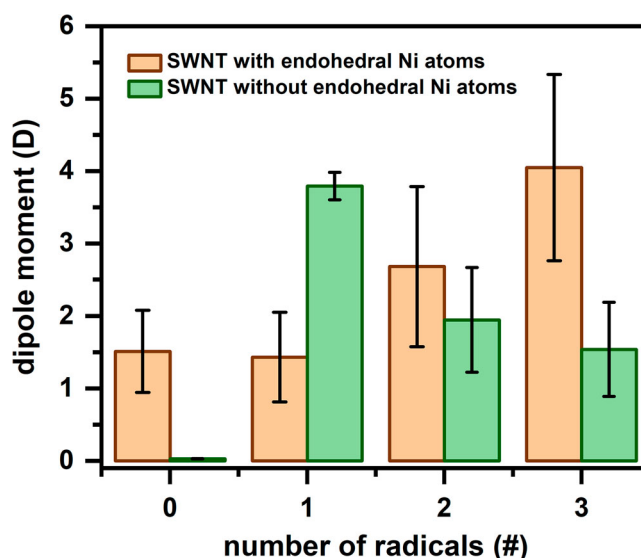


Figure 6. Average dipole moments of pristine/functionalized SWNTs with and without endohedral Ni atoms as a function of the number of functional groups (i.e. -COOH radicals). Associated standard deviations are shown as error bars.

Figure 6). Specifically, the average dipole moments of SWNT with endohedral Ni atoms and its structures functionalized with one, two and three -COOH radicals are 1.513, 1.433, 2.681 and 4.046 D, respectively. As is clear, an increase in the number of functional groups leads to an increase in the dipole moment of SWNT with endohedral Ni atoms, thereby increasing its hydrophilicity. Note that, as mentioned in the Simulation details section, we obtained each dipole moment by averaging their values over 600 MD frames, and thus, it is difficult to elucidate the reason for increased dipole moments by increasing the number of functional groups due to the dynamic evolution of the system (i.e. the positions of atoms change in each MD frame). Nevertheless, we can summarize that filling an SWNT with endohedral Ni atoms and functionalizing it with -COOH radicals increases its dipole moment, thereby increasing its hydrophilicity and thus its solubility in water.

2.1.1.3. Interaction of SWNT with surrounding water. A change in the dipole moment of an SWNT changes its interaction with a polar solvent, such as water. Thus, we evaluated the interaction energies of pSWNT and fSWNT (with and without endohedral Ni atoms) with surrounding water molecules (see Table 2). Note that these energies are calculated in the same way as the binding energy given in formula (1). In other words, the interaction energy between SWNT and water was determined by subtracting the sum of the separately calculated potential energies of SWNT and water from the total potential energy of the system (SWNT + water).

Table 2. Average interaction energies (E_i) of pSWNT and fSWNT with water molecules.

| Number of -COOH radicals | $E_i \pm \Delta E_i$ (eV) | |
|--------------------------|---------------------------|-------------------|
| | SWNT without nickel | SWNT with nickel |
| 0 | -5.29 ± 0.19 | -5.81 ± 0.26 |
| 1 | -5.99 ± 0.30 | -6.72 ± 0.34 |
| 2 | -6.95 ± 0.90 | -12.99 ± 0.40 |
| 3 | -8.76 ± 1.71 | -13.79 ± 0.55 |

As seen from the table, the interaction energy between pSWNT and water molecules is -5.29 eV, and this energy increases with an increase in the number of functional groups in fSWNT without endohedral Ni atoms. In particular, this energy is found to be -5.99 eV, -6.95 eV and -8.76 eV for fSWNT with one, two and three radicals, respectively. The table also shows that the introduction of Ni atoms into the above nanotubes leads to a further increase in the interaction energy of SWNT with water. In particular, the interaction energies of SWNTs with endohedral Ni atoms containing zero, one, two and three radicals are -5.81 , -6.72 , -12.99 , and -13.79 , respectively. Thus, we can conclude that the functionalization of the nanotube increases its interaction with the surrounding aqueous medium, which is further enhanced by the introduction of endohedral Ni atoms into the nanotube. In general, the functionalization of SWNT along with filling it with endohedral Ni atoms enhances its interaction with water, which leads to an increase in its solubility, ultimately reducing its toxicity. It is essential to note that studying the impact of SWNT size (or curvature) and/or the influence of adjacent SWNTs (i.e. SWNT bundles) on the hydrophilicity of both pSWNT and fSWNT (with and without endohedral Ni atoms) is also of significant importance. We intend to consider these aspects in our future investigations.

3. Conclusions

In this research, reactive MD simulations were performed to study the synergistic effect of endohedral Ni atoms and surface functional groups on SWNT hydrophilicity. The ReaxFF force field parameter set used in this study was validated to adequately describe the water environment. The simulation results showed that the binding energy corresponding to a single functional group in SWNT without endohedral Ni atoms remains practically unchanged with an increase in the number of functional groups, whereas it slightly decreases in the case of SWNT with endohedral Ni atoms. Nevertheless, the binding energies of SWNT with endohedral nickel atoms are about 10% higher than the binding energies of SWNT without endohedral nickel atoms, which indicates a stronger binding of functional groups to the surface of SWNT containing encapsulated nickel atoms. The findings also indicated that the introduction of endohedral nickel atoms and the functionalization of SWNT with $-COOH$ radicals lead to an increase in its dipole moments, consequently enhancing the hydrophilicity and subsequent water solubility of SWNT. The interaction energies between SWNT and the surrounding aqueous medium indicated that functionalizing SWNT enhances these energies, and this effect is further amplified when SWNT is filled with endohedral nickel atoms. In general, the combined effect of functionalizing SWNTs and filling them with endohedral nickel atoms improves their interaction with water, resulting in heightened solubility and, ultimately, reduced toxicity.

Acknowledgment

This research work was carried out within the framework of the fundamental project F-FA-2021-512 funded by the Agency for Innovative Development of the Republic of Uzbekistan. Simulations were carried

out using the supercomputer cluster of the Institute of Ion-Plasma and Laser Technologies of the Academy of Sciences of Uzbekistan.

Disclosure statement

No potential conflict of interest was reported by the author(s).

Funding

This work was supported by Agency for Innovative Development of the Republic of Uzbekistan: [Grant Number F-FA-2021-512].

References

- [1] Kasálková NS, et al. Carbon nanostructures, nanolayers, and their composites. *Nanomaterials*. 2021;11(9):2368. doi:10.3390/nano11092368
- [2] Rahman G, et al. An overview of the recent progress in the synthesis and applications of carbon nanotubes. *C-J Carbon Research*. 2019;5(1):3. doi:10.3390/c5010003
- [3] Liu X, et al. Understanding the interaction of single-walled carbon nanotube (SWCNT) on estrogen receptor: a combined molecular dynamics and experimental study. *Ecotoxicol Environ Saf*. 2019;172:373.
- [4] Zamani F, et al. "Nanofibrous and nanoparticle materials as drug-delivery systems." In *Nanostructures for Drug Delivery* 239–270 Elsevier; 2017.
- [5] Kamel M, et al. Assessment of the adsorption mechanism of Flutamide anticancer drug on the functionalized single-walled carbon nanotube surface as a drug delivery vehicle: An alternative theoretical approach based on DFT and MD. *Appl Surf Sci*. 2018;434:492–503.
- [6] Sheikhi M, et al. Adsorption properties of the molecule resveratrol on CNT (8, 0–10) nanotube: geometry optimization, molecular structure, spectroscopic (NMR, UV/Vis, excited state), FMO, MEP and HOMO-LUMO investigations. *J Mol Struct*. 2018;1160:479.
- [7] Lotfi M, et al. Comprehensive quantum chemical insight into the mechanistic understanding of the surface functionalization of carbon nanotube as a nanocarrier with cladribine anticancer drug. *Appl Surf Sci*. 2018;462:720.
- [8] Liu H, et al. Translocation of single-stranded DNA through single-walled carbon nanotubes. *Science*. 2010;327(5961):64.
- [9] Lee CY, et al. Coherence resonance in a single-walled carbon nanotube ion channel. *Science*. 2010;329(5997):1320.
- [10] Geng J, et al. Stochastic transport through carbon nanotubes in lipid bilayers and live cell membranes. *Nature*. 2014;514:612.
- [11] Liang L, et al. DNA fragment translocation through the lipid membrane assisted by carbon nanotube. *Int J Pharm*. 2020;574:118921.
- [12] Yang X, et al. Multi-functionalized single-walled carbon nanotubes as tumor cell targeting biological transporters. *J Nanopart Res*. 2008;10:815.
- [13] De La Zerda A, et al. Carbon nanotubes as photoacoustic molecular imaging agents in living mice. *Nature Nanotech*. 2008;3:557.
- [14] Shi Kam NW, et al. Nanotube molecular transporters: internalization of carbon nanotube–protein conjugates into mammalian cells. *J Am Chem Soc*. 2004;126(22):6850. doi:10.1021/ja0486059
- [15] Warheit DB, et al. Comparative pulmonary toxicity assessment of single-wall carbon nanotubes in rats. *J Toxicol Sci*. 2003;77(1):117. doi:10.1093/toxsci/kfg228
- [16] Karnati KR, et al. Understanding the co-loading and releasing of doxorubicin and paclitaxel using chitosan functionalized single-walled carbon nanotubes by molecular dynamics simulations. *Phys Chem Chem Phys*. 2018;20(14):9389. doi:10.1039/C8CP00124C
- [17] Koh B, et al. Mechanisms of carbon nanotube aggregation and the reversion of carbon nanotube aggregates in aqueous medium. *J Am Chem Soc*. 2014;30(36):10899.

- [18] Scrivens WA, et al. Potent solvents for C₆₀ and their utility for the rapid acquisition of ¹³C NMR data for fullerenes. *Chem Commun.* 1993;15:1207.
- [19] Ruoff RS, et al. Solubility of fullerene (C₆₀) in a variety of solvents. *J Phys Chem.* 1993;97:3379.
- [20] Casey A. Single walled carbon nanotubes induce indirect cytotoxicity by medium depletion in A549 lung cells. *Toxicol Lett.* 2008;179(2):78. doi:10.1016/j.toxlet.2008.04.006
- [21] Shvedova AA, et al. Mechanisms of pulmonary toxicity and medical applications of carbon nanotubes: two faces of janus? *Pharmacol Ther.* 2009;121:192.
- [22] Lam CW, et al. Pulmonary toxicity of single-wall carbon nanotubes in mice 7 and 90 days after intratracheal instillation. *J Toxicol Sci.* 2004;77:126.
- [23] Mananghaya M, et al. Theoretical investigation of the solubilization of COOH-functionalized single wall carbon nanotubes in water. *J Mol Liq.* 2016;215:780.
- [24] Wang R, et al. Cytotoxicity screening of single-walled carbon nanotubes: detection and removal of cytotoxic contaminants from carboxylated carbon nanotubes. *Mol Pharm.* 2011;8(4):1351. doi:10.1021/mp2001439
- [25] Singh R, et al. Binding and condensation of plasmid DNA onto functionalized carbon nanotubes: toward the construction of nanotube-based gene delivery vectors. *J Am Chem Soc.* 2005;127(12):4388. doi:10.1021/ja0441561
- [26] Bianco A, et al. Biomedical applications of functionalised carbon nanotubes. *Chem Commun.* 2005;5:571.
- [27] Prato M, et al. Functionalized carbon nanotubes in drug design and discovery. *Acc Chem Res.* 2008;41(1):60. doi:10.1021/ar700089b
- [28] Kam NWS, et al. Carbon nanotubes as intracellular protein transporters: generality and biological functionality. *J Am Chem Soc.* 2005;127(16):6021. doi:10.1021/ja050062v
- [29] Jain KK. Advances in use of functionalized carbon nanotubes for drug design and discovery. *Expert Opin Drug Discov.* 2012;7(11):1029. doi:10.1517/17460441.2012.722078
- [30] Kiran AR, et al. Carbon nanotubes in drug delivery: focus on anticancer therapies. *J Drug Deliv Sci Technol.* 2020;59:101892.
- [31] Shiozawa H, et al. Nickel clusters embedded in carbon nanotubes as high performance magnets. *Sci Rep.* 2015;5(1):15033. doi:10.1038/srep15033
- [32] Khalilov U, et al. Catalyzed growth of encapsulated carbyne. *Carbon N Y.* 2019;153:1.
- [33] van Duin ACT, et al. ReaxFF: a reactive force field for hydrocarbons. *J Phys Chem A.* 2001;105:9396.
- [34] Yusupov M, et al. Reactive molecular dynamics simulations of oxygen species in a liquid water layer of interest for plasma medicine. *J Phys D: Appl Phys.* 2014;47:025205.
- [35] Khalilov U, et al. Molecular evidence for feedstock-dependent nucleation mechanisms of CNTs. *Nanoscale Horiz.* 2019;4:674.
- [36] Zou C, et al. Molecular dynamics simulations of the effects of vacancies on nickel self-diffusion, oxygen diffusion and oxidation initiation in nickel, using the ReaxFF reactive force field. *Acta Mater.* 2015;83:102.
- [37] Berendsen HJC, et al. Molecular dynamics with coupling to an external bath. *J Chem Phys.* 1984;81(8):3684. doi:10.1063/1.448118
- [38] Peigney A, et al. Specific surface area of carbon nanotubes and bundles of carbon nanotubes. *Carbon N Y.* 2001;39(4):507. doi:10.1016/S0008-6223(00)00155-X
- [39] Mananghaya MR. Adsorption of CO and desorption of CO₂ interacting with Pt (111) surface: a combined density functional theory and Kinetic Monte Carlo simulation. *Adsorption.* 2020; 26:461.
- [40] Jonsson H, et al. Nudged elastic band method for finding minimum energy paths of transitions. In: BJ Berne, G Ciccotti, DF Coker, editor. *Classical and quantum dynamics in condensed phase simulations.* Singapore: World Scientific; 1998. Chapter 16.
- [41] Fogarty JC, et al. A reactive molecular dynamics simulation of the silica-water interface. *J Chem Phys.* 2010;132(17):174704. doi:10.1063/1.3407433
- [42] Berendsen HJC, et al. The missing term in effective pair potentials. *J Phys Chem.* 1987;91:6269.
- [43] Sprik M, et al. Ab initio molecular dynamics simulation of liquid water: comparison of three gradient-corrected density functionals. *J Chem Phys.* 1996;105(3):1142. doi:10.1063/1.471957
- [44] Benedict WS, et al. Rotation-Vibration spectra of deuterated water vapor. *J Chem Phys.* 1956;24(6):1139. doi:10.1063/1.1742731
- [45] Bentwood RM, et al. Studies of intermolecular interactions by matrix isolation vibrational spectroscopy. *J Mol Spectrosc.* 1980;84(2):391. doi:10.1016/0022-2852(80)90031-4
- [46] Clough SA, et al. Dipole moment of water from Stark measurements of H₂O, HDO, and D₂O. *J Chem Phys.* 1973;59:2254.
- [47] Kuchitsu K, et al. Estimation of anharmonic potential constants. II. Bent XY₂ Molecules. *Chem Soc Jpn.* 1965;38:805.
- [48] Badyal YS, et al. Electron distribution in water. *J Chem Phys.* 2000;112:9206. doi:10.1063/1.481541